U. Walzer, R. Hendel. A Geodynamic Model of the Evolution of the Earth's Chemical Mantle Reservoirs. In W. E. Nagel, D. B. Kröner, and M. M. Resch, editors, High Perf. Comp. Sci. Engng. '10 (HLRS), pages 573-592. Berlin, 2011.

A Geodynamic Model of the Evolution of the Earth's Chemical Mantle Reservoirs

Uwe Walzer and Roland Hendel

Abstract A dynamic 3-D spherical-shell model for the chemical evolution of the Earth's mantle is presented. Chemical differentiation, convection, stirring, and thermal evolution constitute an inseparable dynamic system. Our model is based on the solution of the balance equations of mass, momentum, energy, angular momentum, and four sums of the number of atoms of the pairs ^{238}U-^{206}Pb, ^{235}U-^{207}Pb, ^{232}Th-^{208}Pb, and ^{40}K-^{40}Ar. Similar to the present model, the continental crust of the real Earth was not produced entirely at the start of the evolution but developed episodically in batches. The details of the continental distribution of the model are largely stochastic, but the spectral properties are quite similar to the present real Earth. Fig. 6 reveals that the modelled present-day mantle has *no* chemical stratification but we find a marble-cake structure. If we compare the observational results of the present-day proportion of depleted MORB mantle with the model then we find a similar order of magnitude. The MORB source dominates under the lithosphere. In our model, there are nowhere pure unblended reservoirs in the mantle. It is, however, remarkable that, in spite of 4500 Ma of solid-state mantle convection, certain strong concentrations of distributed chemical reservoirs continue to persist in certain volumes, although without sharp abundance boundaries. Section 4 presents results regarding the numerical method, implementation, scalability and performance.

1 Introduction: Geochemical Mantle Resevoirs

Chemical differentiation in the uppermost parts of the silicate shell of the Earth alters the distribution of radioactive elements and volatiles and generates geochemical heterogeneity. On the other hand, convective stirring by solid-state creep diminishes and annihilates these chemical heterogeneities. For example, convection transports and mixes oceanic crust and oceanic mantle lithosphere into the deeper mantle. Where mantle viscosity is high, however, mixing is partly suppressed and chemical signatures tend to be partly

Uwe Walzer · Roland Hendel
Institut für Geowissenschaften, Friedrich-Schiller-Universität, Burgweg 11, 07749 Jena, Germany, e-mail: u.walzer@uni-jena.de; roland.hendel@uni-jena.de

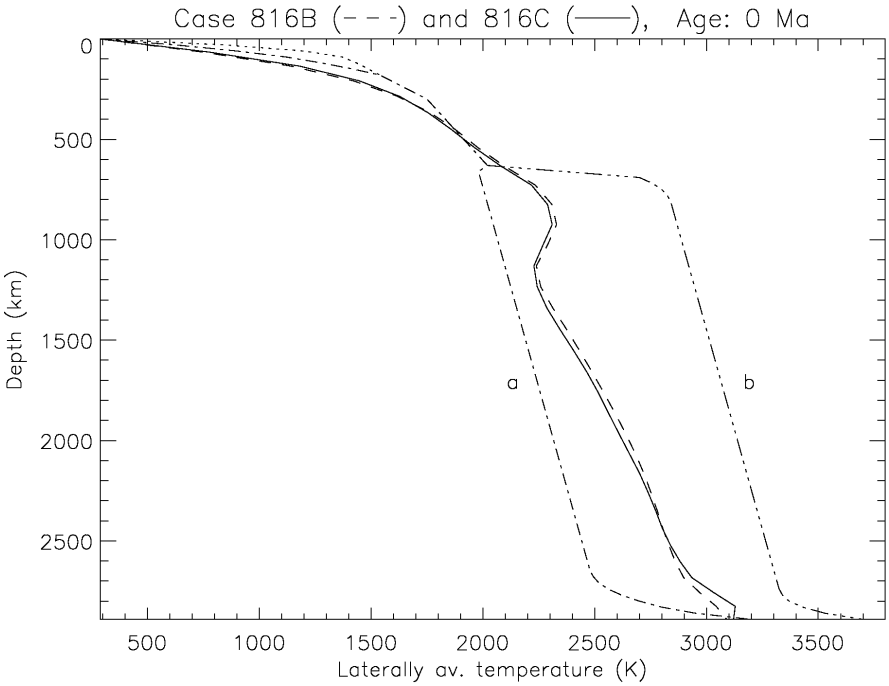

Fig. 1 The laterally averaged temperature of the geological present time as a function of depth for the reference B-run (dashed) and the reference C-run (solid curve) both with a viscoplastic yield stress, $\sigma_y = 120$ MPa, and a viscosity level parameter, $r_n = -0.5$. Cf. Eqs. (1) and (2). A range of realistic mantle geotherms using parameterized models of the mantle's thermal history given by *Schubert et al.* [34] is depicted for comparison. Label a and b signify geotherms of whole-mantle and layered convection, respectively. The dotted line denotes a mid-oceanic ridge geotherm

preserved. Generation, preservation and destruction of mantle heterogeneities are obviously influenced by an interplay among chemical differentiation, convection, and secular cooling. It is evident that the chemical evolution of the mantle cannot be modeled without accounting for the convective process and the mixing it generates. The fact that chemical differentiation causes the distribution of heat-producing elements in the mantle to be non-uniform, in turn, also influences convection. This paper seeks to account for both differentiation and convection/mixing together. The *focus* is the distribution of the MORB source in the Earth's mantle. See also *Hofmann* [13, 14].

In this connection, there are four major questions.

1. How large is the mass ratio of the depleted MORB mantle (DMM) to that part of the mantle which is richer in incompatible elements, yet? MORB denotes the mid-oceanic ridge basalts.
2. Is there a chemical layering, e.g., an upper DMM spherical shell and a lower shell rich in incompatible elements?

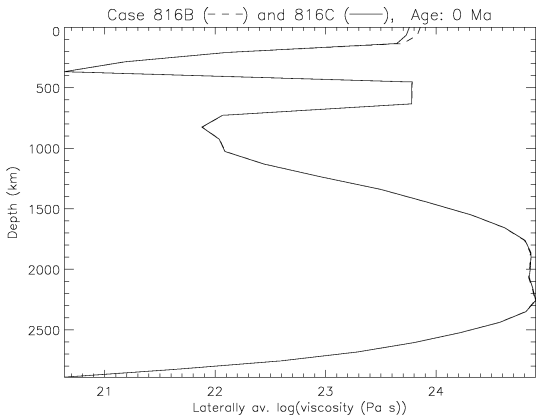

Fig. 2 The laterally averaged shear viscosity of the reference B-run (dashed) and the reference C-run (solid curve) as a function of depth for the present geological time

3. Or are the chemical mantle reservoirs totally mixed by convection?
4. Is the distribution of depleted parts of the mantle like that of pancakes in a matrix or do we observe a marble-cake structure where DMM dominates only in the asthenosphere?

In the *Ogawa* [27] models, chemical stratification develops regardless of the strength of the olivine barrier and lithospheric plates move if the mass exchange through the 660-km discontinuity is not strongly impeded by the olivine barrier. For their case LIHST, the final solution of the compositional distribution is reminiscent of the model by *Kellogg et al.* [20] in regard to its geometry but not to how it arises. Despite large advances in numerical modeling, there is currently no consensus regarding the present-day spatial distribution of chemically distinct reservoirs in the Earth's mantle. The classical chemical two-layer model was a depleted mantle above the 660-km seismic discontinuity and a primordial mantle below it. But many modifications have since been suggested. *Becker et al.* [2] proposed a distribution of the primitive mantle in blobs plus an enriched recycled crust (ERC) at the bottom of the mantle. *Tackley* [37, 38] suggested that enriched piles sit on top of an ERC layer that is at the bottom. Because P-wave and S-wave velocity differences are not correlated deep in the lower mantle [36, 22], these variations cannot be accounted for by temperature differences. So, *Kellogg et al.* [20] proposed a primordial layer at the base of the mantle with an undulating upper surface.

The present picture of the chemistry and dynamics of the mantle is somewhat complex. Moreover, with respect to the provenance of MORB and Oceanic Island Basalts (OIB) there are two different fundamental interpretations.

(a) As illustrative for the first, *Ito and Mahoney* [15, 16] inferred that the MORB and OIB systematics arise from a heterogeneous mantle without large-scale reservoirs. Lower melt fractions and smaller sampling volumes

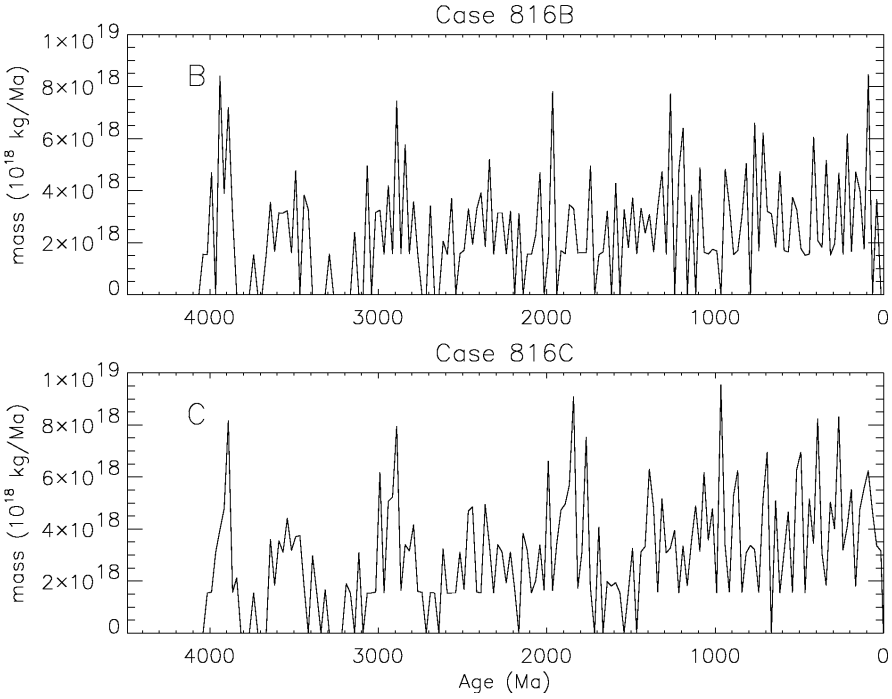

Fig. 3 Time evolution of the juvenile contributions to the total mass of the continents. Comparison of B-run (upper panel) and C-run (lower panel). The rate of the converted continental-tracer mass has been averaged for every 25 Ma and plotted in discretized form. We converted the mass into units of 10^{18}kg/Ma

generate the relatively heterogeneous OIB, whereas larger melt fractions and larger sampling volumes produce the relatively homogeneous MORB. The mean mantle of their model generates less than 30% of the mantle's heat budget so a large heat flow from the core is required. A similar interpretation is that, under slightly different P-T conditions, different degrees of partial melting, and different degrees of homogenization prior to eruption, MORB and OIB can be produced from the same statistical upper mantle assemblage [24, 25, 26, 32].

(b) As illustrative for the second major view, *Kellogg et al.* [19] adopt an extended conventional geochemical reservoir model and conclude that the isotopic differences between MORB and OIB cannot simply be due to differences in sampling volume but must also reflect differences in the source reservoirs and/or the melting processes. They claim to demonstrate that the argument that the absence of samples with a primitive-mantle isotopic signature means an absence of primitive material now in the mantle is not valid.

In the meantime, the theory of geochemical reservoirs has been further refined (*Hofmann* [14]; *Bennett* [3]) such that the reservoirs are no longer

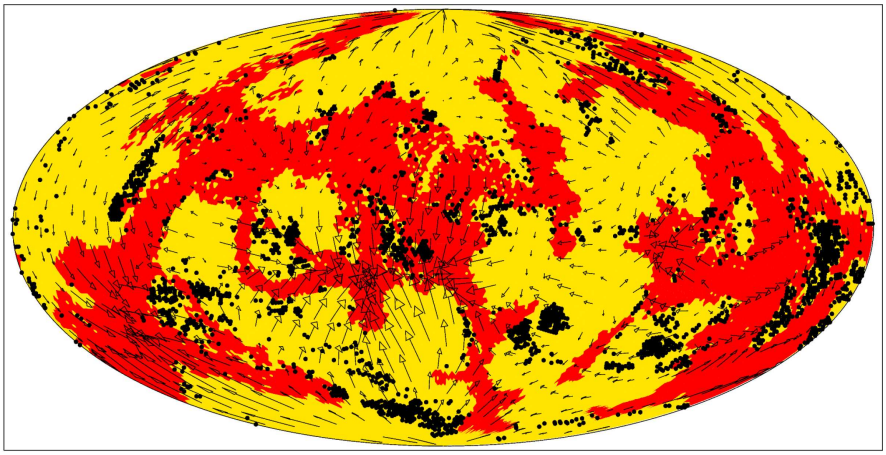

Fig. 4 The distribution of continents (red) and oceanic lithospheric plates (yellow) at the Earth's surface for the geological present time according to the reference B-run. Black dots represent oceanic plateaus. Arrows denote velocity

necessarily understood as separate large-scale volumes. For example, *Stracke et al.* [35] and *Willbold and Stracke* [42] propose a new FOZO similar to the traditional FOZO advanced by *Hart et al.* [12] except that this new FOZO is a small-scale component, ubiquitously dispersed throughout the entire mantle. However, in most *current* reservoir models, the percentages of the reservoirs can systematically vary across the mantle. The existence of sharp chemical boundaries is no longer deemed necessary. We remark that, according to our present dynamical model, the percentage of FOZO in the uppermost part of the mantle should be less than in the lower mantle. This result corresponds with *Wilson's and Spencer's* [43] conclusion that FOZO is the characteristic signal of mantle plumes. Using this conception, the mantle is everywhere heterogeneous and only the mixing ratios of the reservoirs vary. Whether or not such a distributed geochemical reservoir theory is viable is still an open issue. Sections 1 and 2 of [41] give lots of further information regarding the geochemical foundations of our numerical model.

2 Model

We use the numerical model by *Walzer and Hendel* [39] in which the differential equations of infinite Prandtl-number convection within a 3-D spherical-shell mantle are solved using a finite element method. We integrated the chemical differentiation of plateau basalts and continental growth calculat-

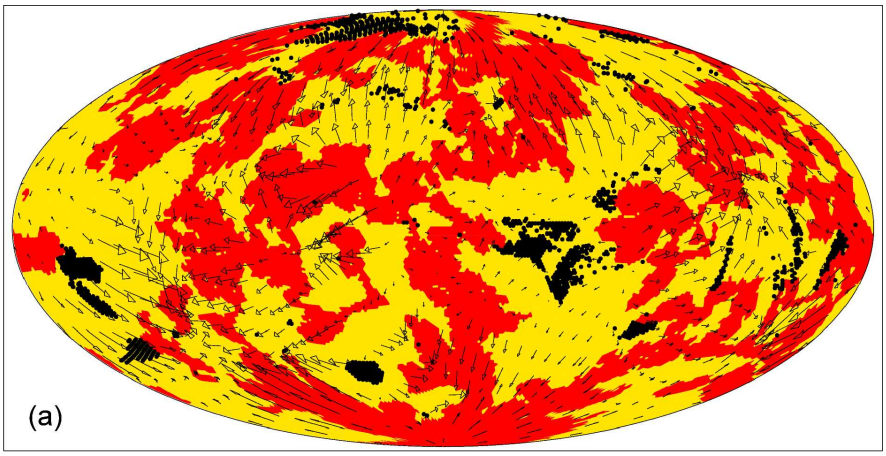

Fig. 5 Continents (red), oceanic lithosphere (yellow) and oceanic plateaus (black dots) for the reference C-run and its neighbors. These C-runs have the same $r_n = -0.50$. First panel, **(a)**, second panel, **(b)**, and third panel, **(c)**, differ among each other only by the yield stress 125, 120 and 115 MPa, respectively

ing the whole thermal history of about 4500 Ma for those times when the mantle creep was mainly dominated by solid-state creep with only a very low percentage of magma chambers. Unlike other mantle-convection papers with continents, our continents are not artificially imposed but evolve by chemical differentiation of which the process has been represented by a tracer approach. A full derivation of the equations and a presentation of the model parameters is given by *Walzer et al.* [41]. Nevertheless, the present companion paper presents exclusively unpublished material.

The viscosity law is based on experimental results of *Karato and Li* [17], *Karato and Wu* [18], and *Li et al.* [23]. Therefore, we assume Newtonian solid-state creep for the Earth's mantle. The shear viscosity, η, is calculated by

$$\eta(r,\theta,\phi,t) = 10^{r_n} \cdot \frac{\exp(c\ \overline{T_m/T_{av}})}{\exp(c\ \overline{T_m/T_{st}})} \cdot \eta_3(r) \cdot \exp\left[c_t \cdot T_m \left(\frac{1}{T} - \frac{1}{T_{av}}\right)\right] \quad (1)$$

where r is the radius, θ the colatitude, ϕ the longitude, t the time, r_n the viscosity-level parameter, T_m the melting temperature, T_{av} the laterally averaged temperature, T_{st} the initial temperature profile, T the temperature as a function of r, θ, ϕ, t. The quantity r_n of the first factor of the right-hand side of Eq. (1) has been used for a stepwise shift of the viscosity profile to vary the averaged Rayleigh number from run to run. The second factor attempts to capture the increase in the viscosity profile resulting from the

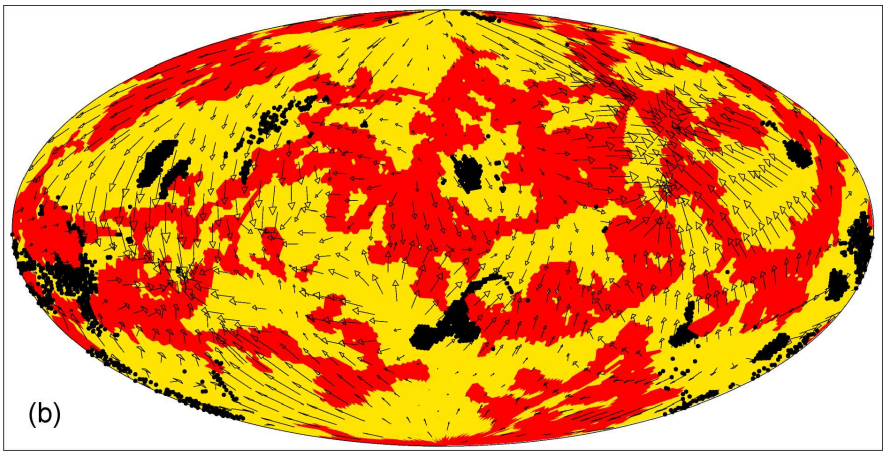

Fig. 5 (Continued)

cooling of the Earth. According to *Yamazaki and Karato* [44], an appropriate value for $MgSiO_3$ perovskite is *c=14*, and for MgO wüstite is *c=10*. So, the lower-mantle c should be somewhere between these two values. For numerical reasons, we are restricted to a value of *c=7*. The quantity $\eta_3(r)$ is the viscosity profile at the initial temperature and for $r_n = 0$. That is, $\eta_3(r)$ describes the dependence of viscosity on pressure and mineral phase. The derivation of $\eta_3(r)$ is provided in *Walzer et al.* [40]. In that paper, we start from a self-consistent theory using the Helmholtz free energy, the Birch-Murnaghan equation of state, the free-volume Grüneisen parameter and *Gilvarry's* [9] formulation of Lindemann's law. The viscosity is calculated as a function of melting temperature provided by Lindemann's law. We use pressure, P, bulk modulus, K, and $\partial K/\partial P$ from the seismic model PREM [8] to obtain the relative variation in radial viscosity. To set the absolute scale of the viscosity profile, we choose $\eta_3 = 3.45 \times 10^{20} Pa \cdot s$ at 367 km depth. This assumption yields an asthenospheric average viscosity of $10^{21} Pa \cdot s$ corresponding to the widely accepted value from postglacial uplift. Because we allow variation of r_n, the exact choice is not so crucial.

For the uppermost 285 km of the mantle (including crust), an effective viscosity, η_{eff}, was implemented where

$$\eta_{eff} = \min\left[\eta(P,T), \frac{\sigma_y}{2\dot{\varepsilon}}\right], \tag{2}$$

where P is pressure and $\dot{\varepsilon}$ is the second invariant of the strain-rate tensor. The quantity σ_y is a viscoplastic yield stress. This introduction of yield stress for the portion of the domain that includes the cold boundary layer allows our

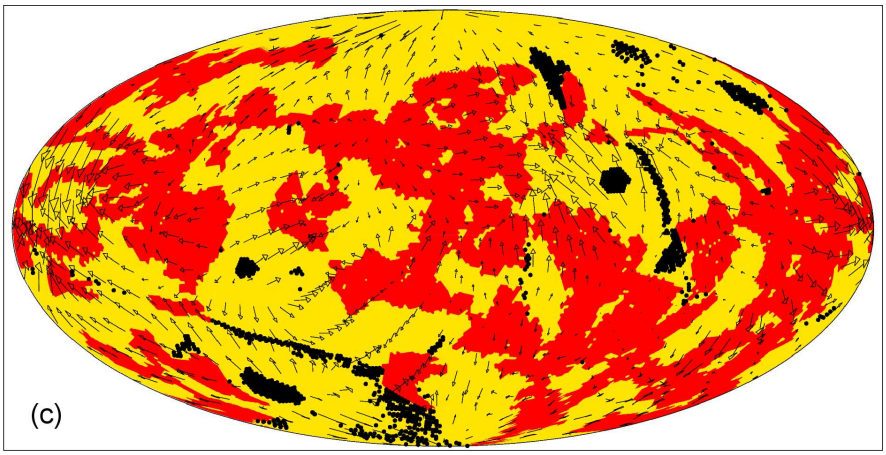

Run 746C ys = 115 MPa rn = −0.50 Time = 4490 Ma
Age = −0.3492 Ma Max vel = 1.879 cm/a Av hor vel = 0.609 cm/a

Fig. 5 (Continued)

model to display plate-like behavior at the surface. Plate-like behavior would not occur without such a rheological treatment and without an asthenosphere.

3 Solution of Numerical Problems Regarding the Tracers Representing the Incompatible Elements in the Earth's Mantle and Results

3.1 General Remarks

Schmalzl [33] demonstrated more than a decade ago that the stirring behavior of the numerical simulation of a convective system depends on whether the simulation is 2-D or 3-D. See also [11]. For 2-D models, side-wall effects can raise additional difficulties since there are no such side walls in the real Earth. Even if we compute in 3-D, but in a Cartesian box, the balance of the atoms of a chemical element is problematic because the area of the core-mantle boundary (CMB) is considerably smaller than the Earth's surface. Therefore we decided to use the 3-D spherical-shell code Terra. As a resolution test, we performed each run twice with differing numbers of tracers. For our basic run (B-run) we used about 10.5 million tracers, and for our comparative run (C-run) we used about 84 million tracers.

The focus of this paper is the generation of continental material via oceanic plateaus by chemical differentiation and the *distribution of reservoirs in the*

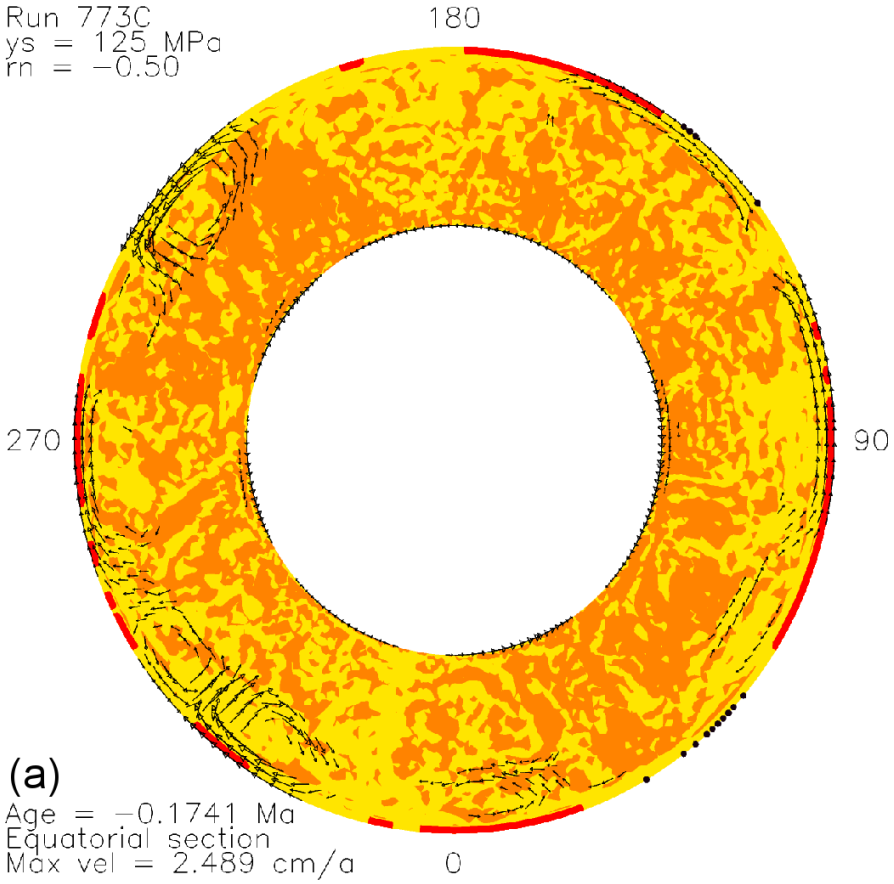

Fig. 6 A comparison of six equatorial sections showing the present-time state of the chemical evolution of incompatible elements of the Earth's mantle. We use a modernized reservoir theory. Cf. Section 1. The depleted MORB mantle (DMM) and a mantle which is rich in incompatible elements, yet, are strongly intermixed. Strongly depleted parts of the mantle which include more than 50% DMM are represented by yellow areas. Relatively rich mantle parts with less than 50% DMM are orange-colored. In general, the yellow-orange boundary does *not* correspond to a discontinuity of the abundances of U,Th,K, etc. The cross sections through the continents are red. Black dots represent the oceanic plateaus. **(a)**The yield stress is 125 MPa, the viscosity-level parameter is -0.50

mantle. This differentiation creates complementary a depleted part of the mantle below the lithosphere. Observational evidence suggests that the contribution of OIBs to continental growth seems to have been considerably larger than that of MORB in the bulk of earlier geological epochs compared to the present [30]. In this paper, we do not *simultaneously* treat all the relevant problems but restrict our attention to that of the chemical differentiation coupled with thermal convection. In particular, we do not include

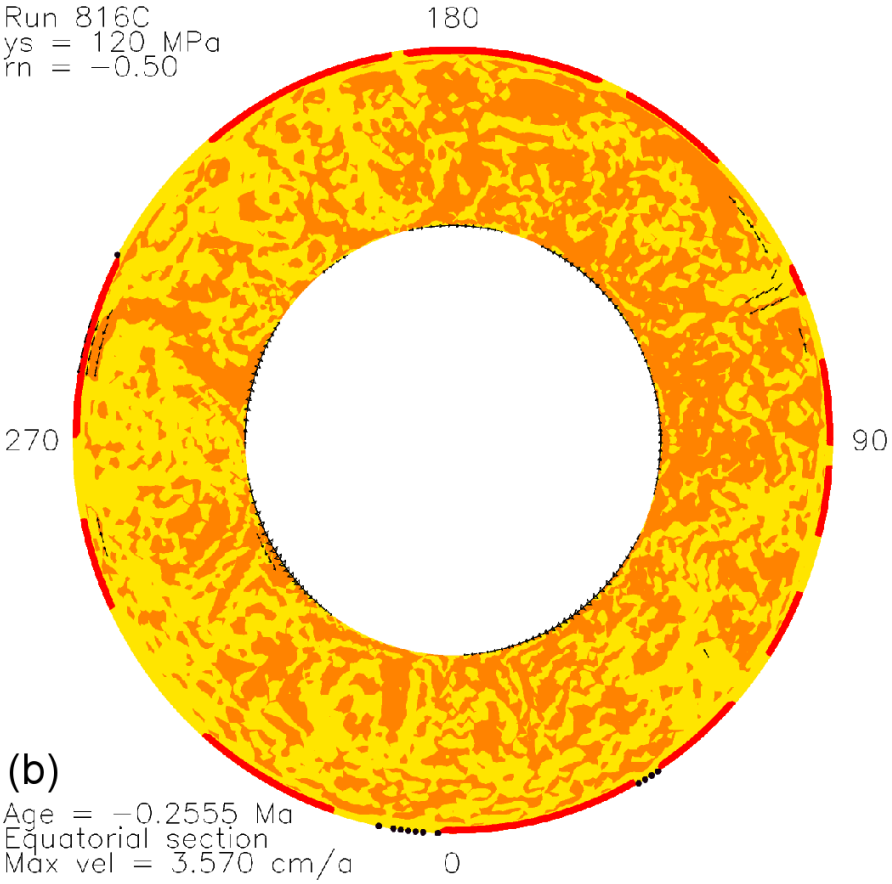

Fig. 6 (b) The yield stress is 120 MPa, the viscosity-level parameter is -0.50. Further Text see (a)

ridge magmatism that produces basaltic oceanic crust and the complementary harzburgitic layer below of it. This has been done by *Ogawa* [28] who, on the other hand, did not include the continent generation. *Ogawa's* and our model complement each other to a certain degree. Therefore, our model certainly does not deal with all relevant aspects of chemical differentiation.

We ran each of our cases to a time of 4.5 billion years to compare our model results with observations of the present Earth. We track the time evolution of Rayleigh number, Ra, Urey number, Ur, and the laterally averaged heat flow, qob, in our runs and compare them with the results of other authors. For this purpose, we vary systematically not only the viscosity-level parameter, r_n, or the temporally averaged Rayleigh number but also the viscoplastic yield stress, called σ_y or ys. We do this not only in that region of $r_n - \sigma_y$ space that is geologically relevant but also outside it to study different solution regimes.

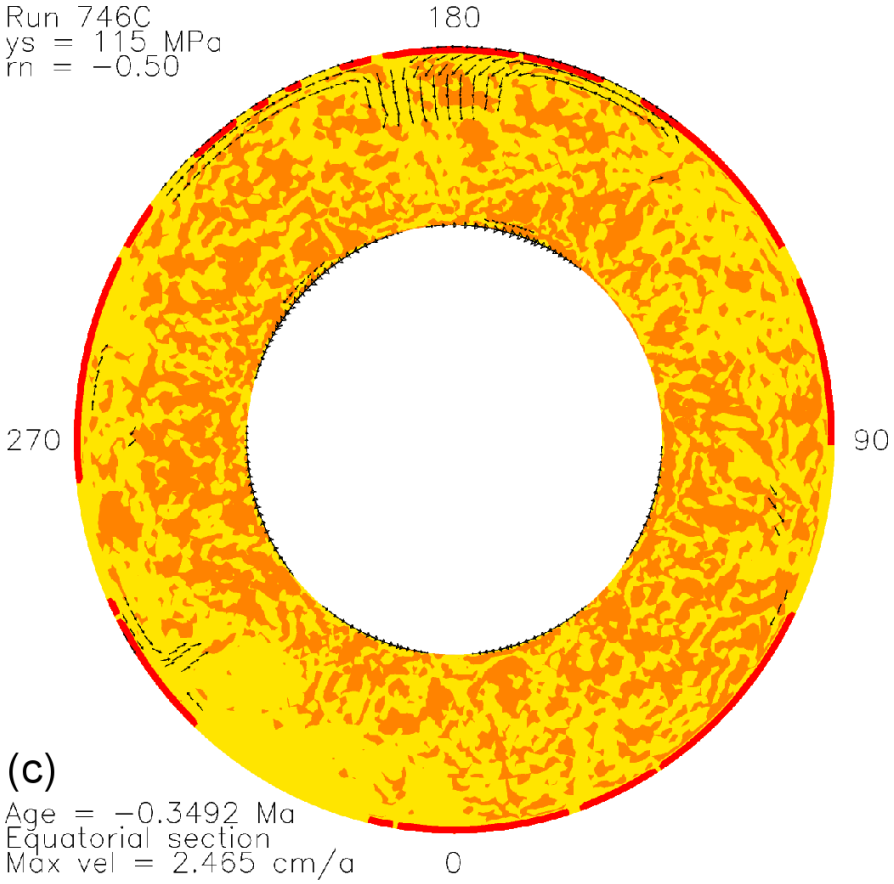

Fig. 6 **(c)** The yield stress is 115 MPa, the viscosity-level parameter is -0.50. Further Text see (a)

3.2 Thermal and Chemical Evolution Using a Pair of Reference Runs

We begin by presenting what we call our two reference runs 816B and 816C. They are representative of the results we obtain in a moderately extensive region of Rayleigh number-yield stress parameter space. Our chosen reference runs are defined by a viscoplastic yield stress, $\sigma_y = 120$ MPa, and a viscosity-level parameter, $r_n = -0.5$. Now, we present the Figures, in each case immediately followed by the corresponding discussion. In Fig. 1, the solid line represents the laterally averaged present-day temperature profile of the C-run, whereas the dashed line displays the corresponding B-run profile. The differences between the two curves are a result of fluctuations produced by the active tracers over the course of the runs. In the beginning of the evolution of

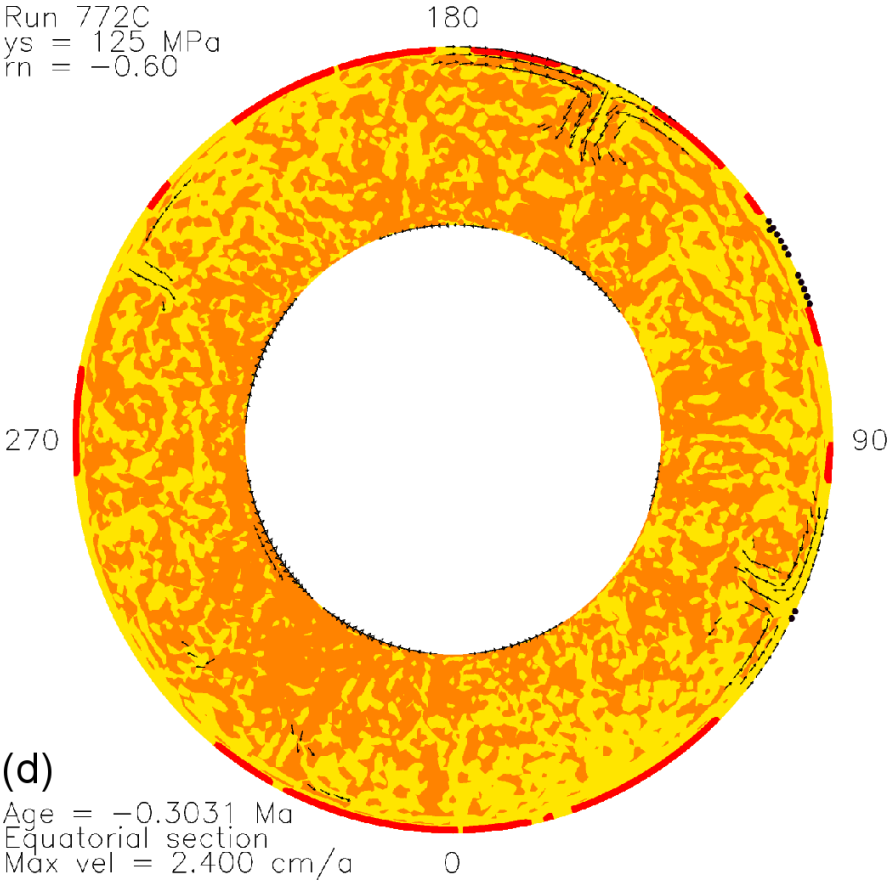

Fig. 6 (d) The yield stress is 125 MPa, the viscosity-level parameter is -0.60. Further Text see (a)

the model, the two curves are nearly identical. Both curves lie closer to the geotherm of the parameterized whole-mantle convection model than to the corresponding layered-convection temperature. This is understandable since the present model displays whole-mantle flow. However, the flow is somewhat impeded by a high-viscosity transition zone and by the endothermic 660-km phase boundary. Therefore, the temperature is slightly augmented, especially immediately beneath the 660-km discontinuity. Our model also includes the full effect of the phase-boundary deflections of the upper mantle.

Fig. 2 shows the laterally averaged viscosity for the present epoch. Deviations between B-run and C-run are distinguishable only for the lithosphere. The definition of the viscosity profiles is given in Section 2. Fig. 3 reveals the production of juvenile continental mass by chemical differentiation of the mantle. The total growth rate within each 25-Ma interval is converted to

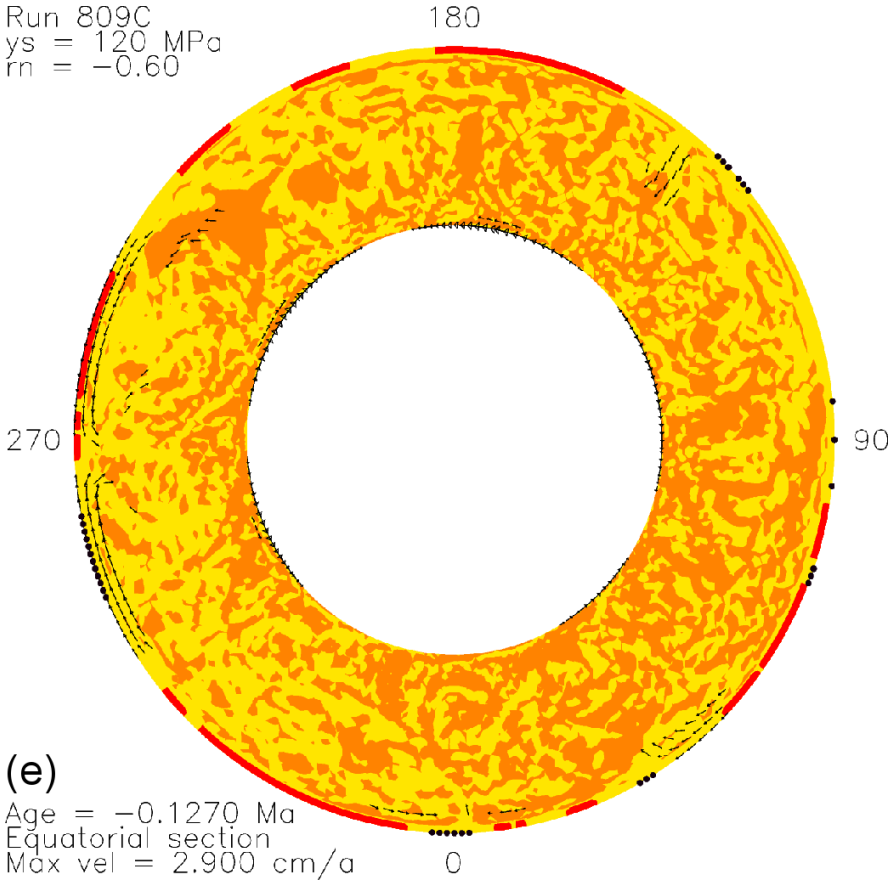

Fig. 6 **(e)** The yield stress is 120 MPa, the viscosity-level parameter is -0.60. Further Text see (a)

10^{18} kg/Ma and graphically represented by a point. The points have been linearly connected. At least in the first half of the evolution, the conversion curves are similar. For this reason and because of the large number of tracers, it is evident that the curves are *not* merely an expression of numerical discretization noise despite the episodic character of the curves. It is obvious that stochastic processes occur both in the real mantle and in the model at bifurcation points etc. That is why it is not to be expected that the two curves of Fig. 3 should exactly coincide and also why the distribution of continents is not predictable in detail *for the present geological epoch*. This applies also for a start with the same slight temperature deviation from the spherically symmetric temperature distribution. We can, however, show that the Fourier spectra of the continent-production curves correspond closely with each other. Notably, the curves of Fig. 3 qualitatively resemble those of ob-

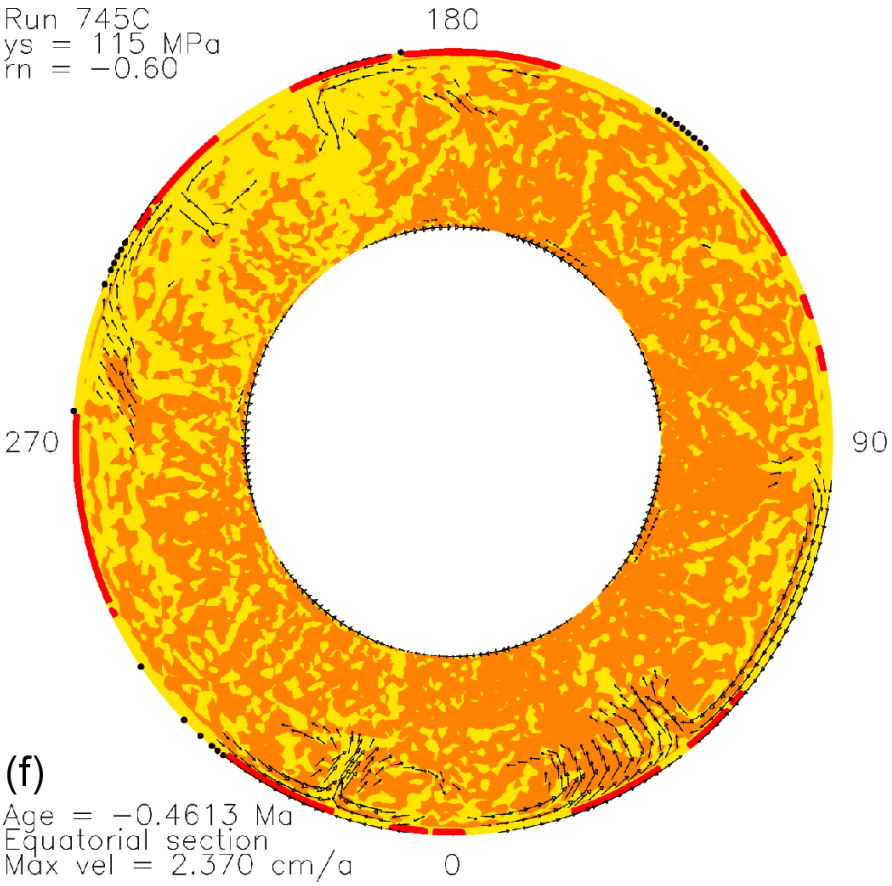

Fig. 6 (f) The yield stress is 115 MPa, the viscosity-level parameter is -0.60. Further Text see (a)

served episodic continental growth ([7], [21]). *Parman* [30] showed that not only the production peaks of OIB but also those of MORB can be correlated to the zircon-age peaks. This observation argues for *episodic* mantle melting and crustal growth. This suggests that, similar to our model, the continental crust was not generated entirely at the beginning but instead evolved episodically in batches, distributed in time over Earth's history.

Fig. 4 reveals the present-time distribution of continents (red) of our reference B-run. The oceanic plateaus (black dots) are carried along by self-consistently generated, moving oceanic lithosphere (yellow). Whenever the plateaus touch a continent they join with it. This is the only additional implementation. At first, we did only visual comparisons between the reference B-run and the reference C-run continental distributions (Fig. 5 (b)). Later we decided to represent both continental distributions in terms of spherical

harmonics.

$$\{A_n^m \quad or \quad B_n^m\} = \frac{\sqrt{2n+1}}{\pi\sqrt{2}} \sqrt{\frac{(n-m)!}{(n+m)!}} \cdot$$
$$\cdot \int_0^{2\pi} \{\cos m\phi \quad or \quad \sin m\phi\} \cdot \left[\int_0^{\pi} f(\theta,\phi) \cdot P_{n,m}(\cos\theta) \cdot \sin\theta \cdot d\theta \right] d\phi, \quad (3)$$

respectively, where $f(\theta,\phi)$ is 1 for continents and 0 for oceanic lithosphere. While the individual coefficients A_n^m or B_n^m depend on the position of the pole of the grid (θ,ϕ), the quantity h_n^* given by

$$h_n^* = \frac{\sqrt{n\cdot(n+1)}}{2} \cdot \left\{ \sum_{m=0}^{n} \left[(A_n^m)^2 + (B_n^m)^2 \right] \right\}^{1/2} \quad (4)$$

is orientation-independent. We find the h_n^*-spectra of B-run and C-run to be similar. We conclude therefore that, whereas the details of the continental distribution are largely stochastic, the spectral properties are quite similar.

3.3 Continents and Mantle Inhomogeneities

Fig. 5 shows that, not so much for the early Earth evolution but for the geological present time, the distribution of continents and velocity vectors of the plates vary for only a slight variation of input parameters, in this case the yield stress, σ_y. A detail in Fig. 5(c) is a convergent plate boundary displaying an aggregation of oceanic plateaus along a zone of an ocean-ocean collision. Such a phenomenon, of course, requires previous generation of oceanic plateaus on those plates that are moving toward the convergent zone. In these models, of course, it is only the h_n^*-spectrum and not such details that is predictable. The same is also likely to be applicable to the Earth's mantle. We are not aware of other papers on spherical-shell mantle convection in which continents evolve entirely as a consequence of physical laws rather than simply being applied to the surface.

Six different cases of the equatorial section of the distribution of ubiquitously dispersed geochemical reservoirs (cf. last paragraph of Section 1) for the present epoch are given by Fig. 6. The second panel corresponds to the reference C-run. In the first three panels of Fig. 6, the viscosity-level parameter is kept constant, namely, $r_n = -0.50$. The first panel corresponds to a yield stress of 125 MPa, the second one to 120 MPa, and the third panel to 115 MPa. So, these three panels correspond to the three continental distributions of Fig. 5. The panels (d) to (f) of Fig. 6 correspond to the same succession of yield-stress values but for $r_n = -0.60$. As implied by Eq. (1),

this means that the viscosity of this second triad is somewhat lower. Depleted parts of the mantle with more than 50% depleted MORB mantle are depicted in yellow. DMM dominates near the surface because DMM is generated near the surface. The depleted, "yellow" material is subducted jointly with the high-viscosity surface plates into the mantle. When cut crosswise by the equatorial section, a partially disintegrated slab is visible as a yellow stripe. It is remarkable that, in spite of 4500 Ma of solid-state mantle convection, chemical reservoirs continue to persist, although without sharp concentration boundaries. In our model there are nowhere pure unblended reservoirs, and this may also be true of the Earth's mantle. DMM predominates immediately below the continents (red) and beneath the oceanic lithosphere. This is a realistic feature of the model since where the real oceanic lithosphere is rifted, MORB magma is formed by decompression melting. The MORB source (DMM) is not only depleted in incompatible elements but also relatively homogenized. It is homogenized not only with respect to its major geochemical components (SiO_2, MgO, FeO, Al_2O_3, CaO) (*Palme and O'Neill* [29]) but also with respect to isotope ratios $^{87}Sr/^{86}Sr$, $^{143}Nd/^{144}Nd$, $^{206}Pb/^{204}Pb$, $^{207}Pb/^{204}Pb$ and $^{208}Pb/^{204}Pb$. As a consequence, the standard deviation of these isotope ratios and of the major element compositions is small for MORBs in comparison to OIBs (*Allègre and Levin* [1]) although *Hofmann* [14] has modified this conclusion somewhat. Fig. 6 represents a marble-cake mantle, similar to what was suggested by *Coltice and Ricard* [6] and *Becker et al.* [2]. It is remarkable that the yellow-orange boundary does not produce simply connected volumes. There is no clear chemical stratification for the present. The present-day proportion of DMM in the real Earth's mantle is not exactly known. Estimates depend on which element is used and its assumed abundance in CC and DMM. If samarium and neodymium are not so extremely enriched in CC, then smaller volumes of DMM are possible. Calculations using Cs, Rb, Th and K suggest 50% of the mantle is DMM. *Bennett* [3] estimated that between 30% and 60% of the mantle is depleted if an intermediate degree of depletion of DMM is assumed. *Hofmann* [14] deduced a depleted reservoir of the mantle between 30% and 80%. If we compare these observational results with the first three panels of Fig. 6, i.e., with the reference C-run and its neighbors, we conclude that the yellow, depleted proportions are of the right order of magnitude. In the model, DMM prevails everywhere immediately under the oceanic or continental lithosphere. So, it is understandable why, as a rule, MORB is generated at sites of rifting of the oceanic lithosphere.

4 Numerical Method, Implementation, Scalability, and Performance

We treat the mantle as a thick spherical shell. The grid for this domain is constructed by projection of the edges of a regular icosahedron onto concentric spherical shell surfaces with different radial distances from the center. These surfaces subdivide the mantle into thin shells. A first step of grid refinement consists of bisecting the edges of the resulting spherical triangles into equal parts. Connecting the new points with great circles, we obtain four smaller triangles from each starting triangle. The process can be repeated by successive steps to obtain a grid with the desired horizontal resolution. We replicate the resulting almost uniform triangular grid at different radii to generate the 3-D grid for a spherical shell. We can use different formulae for the distribution of the radial distances of the spherical grid surfaces. Here, we used exclusively a radially nearly equidistant grid with a superposed sinoidal half-wave length to refine the grid near the upper and lower boundaries of the spherical shell. The Navier-Stokes equations as well as pressure and creeping velocity are discretized using finite elements. We apply piecewise linear basis functions for the creeping velocity and either piecewise constant or piecewise linear basis functions for the pressure. We solve the equations for pressure and velocity simultaneously by a Schur-complement conjugate-gradient iteration [31]. This is a further development of an Uzawa algorithm. We solve the energy equation using an iterative multidimensional positive-definite advection-transport algorithm with explicit time steps (*Bunge and Baumgardner* [4]). Within the Ramage-Wathen procedure, the resulting equation systems are solved by a multigrid procedure that utilizes radial line Jacobi smoothing. In the multigrid procedure, prolongation and restriction are handled in a matrix-dependent manner. In this way, it is possible to handle the strong variations and jumps of the coefficients associated with the strong viscosity gradients (*Yang* [45]). For the formulation of chemical differentiation, we modified a tracer module developed by Dave Stegman. This module contains a second-order Runge-Kutta procedure to move the tracer particles in the velocity field. Each tracer carries the abundances of the radionuclides. In this sense, tracers are active attributes which determine the heat production rate per unit volume that varies with time and position. For convergence tests we compared the results of runs with 1 351 746 and 10 649 730 grid points. The deviations concerning Rayleigh number, Nusselt number, Urey number, and the laterally averaged surface heat flow, *qob*, were smaller than 0.5 %. Benchmark tests of the Terra code [5, 10] showed deviations of less than 1.5 %. Terra is parallelized by domain decomposition according to the dyadic grid refinement and using explicit message passing (MPI). In Table 1 we present measurements of scalability and performance. Using the performance measuring tool `jobperf`, we obtained an average of 1201 MFlop/s with 8 processors, 1116 MFlop/s with 32 processors, and 935 MFlop/s with 128 processors, re-

spectively. In both resolutions the speedup was almost linear, in some cases slightly superlinear due to cache usage. With the high resolution, at least 4 processors are necessary to make efficient use of the cache memory.

Table 1 CPU-time, walltime and speedup for runs with 100 time steps on 1 351 746 nodes (a) and on 10 649 730 nodes (b). For comparison, Speedup (b) for 4 processors has been deliberately set to 4.00.

Procs	CPU-time (a)	Walltime (a)	Speedup (a)	CPU-time (b)	Walltime (b)	Speedup (b)
1	00:27:13	00:27:17	1.00			
4	00:29:12	00:07:33	3.61	05:01:23	01:16:09	4.00
8	00:26:08	00:03:31	7.76	04:53:26	00:37:32	8.12
16	00:25:36	00:02:02	13.42	05:08:51	00:19:35	15.69
32	00:21:52	00:01:02	26.40	04:34:40	00:09:11	33.17
64				05:43:25	00:05:36	54.39
128				05:34:24	00:03:04	100.42

For further tasks, we need an augmentation of grid resolution by a factor of ten in each of the three directions. To run such kind of jobs, a high number of processors, in the order of 10000, is necessary. Up to now, the particle module was the bottleneck of our code. Some parts of this module were not parallelized. But now this task has been solved.

Acknowledgements

We kindly acknowledge the confidential cooperation with John Baumgardner, Markus Müller, and Christoph Köstler. We are very thankful for Dave Stegman for providing his particle code. Furthermore, we thank for the use of supercomputing facilities at SCC Karlsruhe and LRZ München. This work was supported by the Deutsche Forschungsgemeinschaft under grants WA 1035/5-3 and KL 495/16-1.

References

1. C. J. Allègre and E. Levin. Isotopic systems and stirring times of the Earth's mantle. *Earth Planet. Sci. Lett.*, 136:629–646, 1995.
2. T. W. Becker, J. B. Kellogg, and R. J. O'Connell. Thermal constraints on the survival of primitive blobs in the lower mantle. *Earth Planet. Sci. Lett.*, 171:351–365, 1999.
3. V. C. Bennett. Compositional evolution of the mantle. In R. W. Carlson, editor, *Treatise on Geochemistry, Vol.2: The Mantle and the Core*, pages 493–519. Elsevier, Amsterdam, 2003.
4. H.-P. Bunge and J. R. Baumgardner. Mantle convection modelling on parallel virtual machines. *Computers in Physics*, 9:207–215, 1995.

5. H.-P. Bunge, M. A. Richards, and J. R. Baumgardner. A sensitivity study of three-dimensional spherical mantle convection at 10^8 Rayleigh number: Effects of depth-dependent viscosity, heating mode and an endothermic phase change. *J. Geophys. Res.*, 102:11991–12007, 1997.
6. N. Coltice and Y. Ricard. On the origin of noble gases in mantle plumes. *Phil. Trans. Royal Soc. A: Math. Phys. Engng. Sci.*, 360:2633–2648, 2002.
7. K. C. Condie. Episodic continental growth and supercontinents: a mantle avalanche connection? *Earth Planet. Sci. Lett.*, 163:97–108, 1998.
8. A. M. Dziewonski and D. L. Anderson. Preliminary reference Earth model. *Phys. Earth Planet. Int.*, 25:297–356, 1981.
9. J. J. Gilvarry. The Lindemann and Grüneisen laws. *Phys. Rev.*, 102:307–316, 1956.
10. G. A. Glatzmaier. Numerical simulations of mantle convection: Time-dependent, three-dimensional, compressible, spherical shell. *Geophys. Astrophys. Fluid Dyn.*, 43:223–264, 1988.
11. K.-D. Gottschaldt, U. Walzer, R. Hendel, D. R. Stegman, J. R. Baumgardner, and H.-B. Mühlhaus. Stirring in 3-d spherical models of convection in the Earth's mantle. *Philosophical Magazine*, 86:3175–3204, 2006.
12. S. R. Hart, E. H. Hauri, L. A. Oschmann, and J. A. Whitehead. Mantle plumes and entrainment: Isotopic evidence. *Science*, 256:517–520, 1992.
13. A. W. Hofmann. Chemical differentiation of the Earth: The relationship between mantle, continental crust and oceanic crust. *Earth Planet. Sci. Lett.*, 90:297–314, 1988.
14. A. W. Hofmann. Sampling mantle heterogeneity through oceanic basalts: Isotopes and trace elements. In R. W. Carlson, editor, *Treatise on Geochemistry, Vol.2: The Mantle and the Core*, pages 61–101. Elsevier, Amsterdam, 2003.
15. G. Ito and J. J. Mahoney. Flow and melting of a heterogeneous mantle: 1. Method and importance to the geochemistry of ocean island and mid-ocean ridge basalts. *Earth Planet. Sci. Lett.*, 230:29–46, 2005.
16. G. Ito and J. J. Mahoney. Flow and melting of a heterogeneous mantle: 2. Implications for a chemically nonlayered mantle. *Earth Planet. Sci. Lett.*, 230:47–63, 2005.
17. S.-I. Karato and P. Li. Diffusion creep in perovskite: implications for the rheology of the lower mantle. *Science*, 255:1238–1240, 1992.
18. S.-I. Karato and P. Wu. Rheology of the upper mantle: a synthesis. *Science*, 260:771–778, 1993.
19. J. B. Kellogg, S. B. Jacobsen, and R. J. O'Connell. Modeling the distribution of isotopic ratios in geochemical reservoirs. *Earth Planet. Sci. Lett.*, 204:183–202, 2002.
20. L. H. Kellogg, B. H. Hager, and R. D. van der Hilst. Compositional stratification in the deep mantle. *Science*, 283:1881–1884, 1999.
21. A. I. S. Kemp, C. J. Hawkesworth, B. A. Paterson, and P. D. Kinny. Episodic growth of the Gondwana supercontinent from hafnium and oxygen isotopes in zircon. *Nature*, 439:580–583, 2006.
22. B. L. N. Kennett, S. Widiyantoro, and R. D. van der Hilst. Joint seismic tomography for bulk sound and shear wave speed in the Earth's mantle. *J. Geophys. Res.*, 103:12469–12484, 1998.
23. P. Li, S.-I. Karato, and Z. Wang. High-temperature creep in fine-grained polycristalline $CaTiO_3$, an analogue material of $(Mg,Fe)SiO_3$ perovskite. *Phys. Earth Planet. Int.*, 95:19–36, 1996.
24. A. Meibom and D. L. Anderson. The statistical upper mantle assemblage. *Earth Planet. Sci. Lett.*, 217:123–139, 2003.
25. A. Meibom, N. H. Sleep, K. Zahnle, and D. L. Anderson. Models for noble gases in mantle geochemistry: Some observations and alternatives. In G. R. Foulger et al., editors, *Plumes, Plates and Paradigms*, volume 388, pages 347–363. Geological Society of America Special Paper, Boulder, Colorado, 2005.

26. J. P. Morgan and W. J. Morgan. Two-stage melting and the geochemical evolution of the mantle: a recipe for mantle plum-pudding. *Earth Planet. Sci. Lett.*, 170:215–239, 1999.
27. M. Ogawa. Chemical stratification in a two-dimensional convecting mantle with magmatism and moving plates. *J. Geophys. Res.*, 108(B12):2561, 2003.
28. M. Ogawa. Superplumes, plates, and mantle magmatism in two-dimensional numerical models. *J. Geophys. Res.*, 112:B06404, 2007.
29. H. Palme and H. S. C. O'Neill. Cosmochemical estimates of mantle composition. In R. W. Carlson, editor, *Treatise on Geochemistry, Vol.2: The Mantle and the Core*, pages 1–38. Elsevier, Amsterdam, 2003.
30. S. W. Parman. Helium isotopic evidence for episodic mantle melting and crustal growth. *Nature*, 446:900–903, 2007.
31. A. Ramage and A. J. Wathen. Iterative solution techniques for finite element discretizations of fluid flow problems. In *Proceedings of the Copper Mountain Conference on Iterative Methods*, volume 1, Copper Mountain, Colorado, 1992.
32. J. F. Rudge, D. McKenzie, and P. H. Haynes. A theoretical approach to understanding the isotopic heterogeneity of mid-ocean ridge basalt. *Geochim. Cosmochim. Acta*, 69(15):3873–3887, 2005.
33. J. Schmalzl. Mixing properties of thermal convection in the earth's mantle. *Geologica Ultraiectina*, 140:104 pp., 1996.
34. G. Schubert, D. L. Turcotte, and T. R. Olson. *Mantle Convection in the Earth and Planets*. Cambridge Univ. Press, Cambridge, UK, 2001.
35. A. Stracke, A. W. Hofmann, and S. R. Hart. FOZO, HIMU and the rest of the mantle zoo. *Geochem. Geophys. Geosys.*, 6:Q05007, 2005.
36. W.-J. Su and A. M. Dziewonski. Simultaneous inversion for 3-D variations in shear and bulk velocity in the mantle. *Phys. Earth Planet. Int.*, 100:135–156, 1997.
37. P. J. Tackley. Three-dimensional simulations of mantle convection with a thermochemical basal boundary layer: D"? In M. Gurnis et al., editors, *The Core-Mantle Boundary Region, Geodyn. Ser., vol. 28*, pages 231–253. AGU, Washington, D. C., 1998.
38. P. J. Tackley. Mantle convection and plate tectonics: Towards an integrated physical and chemical theory. *Science*, 288:2002–2007, 2000.
39. U. Walzer and R. Hendel. Mantle convection and evolution with growing continents. *J. Geophys. Res.*, 113:B09405, doi:10.1029/2007JB005459, 2008.
40. U. Walzer, R. Hendel, and J. Baumgardner. The effects of a variation of the radial viscosity profile on mantle evolution. *Tectonophysics*, 384:55–90, 2004.
41. U. Walzer, R. Hendel, and J. Baumgardner. Whole-mantle convection, continent generation, and preservation of geochemical heterogeneity. In W. E. Nagel, D. B. Kröner, and M. M. Resch, editors, *High Perf. Comp. Sci. Engng. '07*, pages 603–645. Springer, Berlin, 2008.
42. M. Willbold and A. Stracke. Trace element composition of mantle end-members: Implications for recycling of oceanic and upper and lower continental crust. *Geochem. Geophys. Geosys.*, 7:Q04004, 2006.
43. M. Wilson and E. A. Spencer. The origin and evolution of the fozo/prema and himu mantle components - the carbonatite perspective. http://www.geo.uw.edu.pl/ERASMUS/files/wilson3.ppt, 2003.
44. D. Yamazaki and S.-I. Karato. Some mineral physics constraints on the rheology and geothermal structure of the Earth's lower mantle. *Am. Min.*, 86:385–391, 2001.
45. W.-S. Yang. *Variable viscosity thermal convection at infinite Prandtl number in a thick spherical shell*. PhD thesis, University of Illinois, Urbana-Champaign, 1997.